TU Delft

Delft University of Technology

Document Version
Final published version

Licence
CC BY

Citation (APA)
Fasching, L., Lian, J. Z., Cucurachi, S., & Rwei, A. Y. (2026). A Sustainable-by-Design Wearable Sweat Sensor via Compostable Microfluidics and Laser-Induced Graphene Electrodes for Real-Time Monitoring of Physical Exercise. *ACS Sustainable Chemistry and Engineering*, *14*(40), 18238-18247. https://doi.org/10.1021/acssuschemeng.6c07506

Important note
To cite this publication, please use the final published version (if applicable).
Please check the document version above.

Copyright
In case the licence states “Dutch Copyright Act (Article 25fa)”, this publication was made available Green Open Access via the TU Delft Institutional Repository pursuant to Dutch Copyright Act (Article 25fa, the Taverne amendment). This provision does not affect copyright ownership.
Unless copyright is transferred by contract or statute, it remains with the copyright holder.

Sharing and reuse
Other than for strictly personal use, it is not permitted to download, forward or distribute the text or part of it, without the consent of the author(s) and/or copyright holder(s), unless the work is under an open content license such as Creative Commons.

Takedown policy
Please contact us and provide details if you believe this document breaches copyrights.
We will remove access to the work immediately and investigate your claim.

This work is downloaded from Delft University of Technology.

ACS Sustainable Chemistry & Engineering

pubs.acs.org/ascecg

Open Access

This article is licensed under CC-BY 4.0

Research Article

A Sustainable-by-Design Wearable Sweat Sensor via Compostable Microfluidics and Laser-Induced Graphene Electrodes for Real-Time Monitoring of Physical Exercise

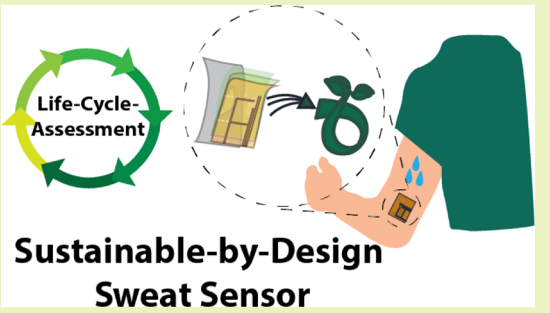
Lena Fasching,° Justin Z. Lian,° Stefano Cucurachi, and Alina Y. Rwei*

Cite This: *ACS Sustain. Chem. Eng.* 2026, 14, 18238−18247

Read Online

ACCESS | Metrics & More | Article Recommendations | Supporting Information

ABSTRACT: The growing demand for non-invasive, real-time health monitoring has accelerated the development of wearable sweat sensors. However, most existing platforms rely on resource-intensive, non-recyclable materials and fabrication processes that impose a significant environmental burden. Here, we present a fully biodegradable, sustainable-by-design wearable sweat sensor that integrates environmentally conscious material selection, scalable fabrication processes, and robust on-body performance, while quantitatively evaluating sustainability through a dual-level life cycle assessment (LCA). The sensor features laser-induced graphene (LIG) electrodes directly engraved onto biodegradable chitosan/paper substrates and a compostable microfluidic platform that passively transports sweat across impedimetric total ionic strength and sweat-rate sensors. In vitro characterization demonstrated ionic strength monitoring across 1–200 mM with a sensitivity of 70 μS/log(mM), and sweat-rate sensing over 0.5–5 μL min^{-1}. On-body exercise measurements demonstrated continuous sweat-rate monitoring, while ionic strength was tracked off-body using collected sweat samples. A dual-level LCA at the whole-device and electrode levels showed consistently reduced environmental impacts compared with conventional PDMS- and metal-based sensor designs across EF 3.1 impact categories. By embedding sustainability at the design stage, this work establishes a pathway toward wearable biosensors with substantially reduced environmental footprints while maintaining functionality.



KEYWORDS: *wearable biosensors, sweat sensing, biodegradable electronics, laser-induced graphene, sustainable microfluidics, life cycle assessment*

INTRODUCTION

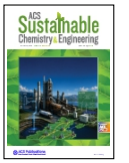
Wearable sweat sensors are gaining significant attention for enabling real-time, non-invasive insights into physiological conditions through painless, non-invasive sampling while reflecting hydration status, electrolyte balance, and a wide range of biomarkers.[1,2] Yet, despite their advantages, the environmental impact of wearable sensing technologies has received insufficient attention.

Life cycle assessments of representative wearable healthcare devices report global warming impacts of 1.1–6.1 kg CO_2-equivalent per unit, with demand projected to increase 42-fold by 2050, reaching nearly 2 billion devices annually. This growth could generate approximately 3.4 Mt CO_2-equivalent emissions, alongside increased ecotoxicity and electronic waste.[3]

These sustainability challenges stem from both material choices and fabrication processes. Most reported devices incorporate precious or rare-metal electrodes-including Au, Pt, and Ag/AgCl-and rely on cleanroom-based fabrication techniques such as photolithography and thin-film deposition,[3−7] which carry considerable embodied energy and resource costs. Substrate and microfluidic components are predominantly based on polydimethylsiloxane (PDMS) and related synthetic polymers that are neither recyclable nor biodegradable.[8,9]

Recent efforts have explored more sustainable materials and fabrication strategies by replacing conventional metal electrodes with carbon-based alternatives and utilizing adhesive-based microfluidic architectures.[10−12] Laser-induced graphene (LIG) has become a promising electrode material, as it can be directly patterned onto various carbon-based substrates.[13] This straightforward fabrication process opened a route to fabricate electrodes on biodegradable substrates such as chitosan[14,15] or paper,[16] while providing high electrical conductivity, flexibility, and biocompatibility.[14−16] Similarly, adhesive-based microfluidics offer a simple, scalable approach for passive sweat collection without requiring molded elastomeric components.[10]

Received: June 26, 2026
Revised: September 14, 2026
Accepted: September 16, 2026
Published: September 21, 2026



ACS Publications

© 2026 The Author(s). Published by American Chemical Society

Downloaded from pubs.acs.org/ascecg/article-pdf/14/40/18238/6858153/sc-2026-07506n.pdf by TU DELFT user on 27 October 2026

The aforementioned studies, however, either were conducted in simplified, protein-free artificial sweat and isolated sensing layers,[14,16] or incorporated limited sustainability considerations that covered only the sensing layer and not the device level.[17] Many designs, at the device level, still depend on conventional polymer substrates, non-recyclable electrode passivation, and non-biodegradable device architectures[10,12,17] and, in most cases, the claimed environmental benefits were not substantiated through quantitative life cycle assessment.[11,12,14−16,18] Consequently, a key challenge remains the development of a fully integrated, sustainable sensing device that fully replaces petrochemical-based materials and thin-film metal electrodes with biodegradable alternatives, while maintaining on-body sensing performance and validating environmental advantages through quantitative LCA studies.

Here, we present a fully biodegradable wearable sweat sensor in which material selection and fabrication strategy serve as the primary design drivers, with functionality demonstrated via sweat rate and ionic strength monitoring as a proof-of-concept, alongside a dual-level LCA to assess environmental impact. In line with sustainable-by-design principles, material selection was restricted to fully biodegradable components, including a chitosan/paper-based substrate, with LIG replacing conventional thin-film metal electrodes. The device's sweat-handling microfluidic system was constructed from a compostable adhesive based on polylactic acid (PLA) and natural rubber, with laser-cut channels enabling passive and controlled sweat transport. As proof-of-concept, this platform uses state-of-the-art designs for impedimetric total ionic strength and sweat-rate sensing,[5,6] aiming for continuous sweat analysis during physical activity. We validated device sweat rate monitoring performance through on-body measurements during exercise and through off-body total ionic strength testing with freshly collected human sweat. The environmental advantages of the selected material system were quantified using a dual-level comparative life cycle assessment (LCA) spanning material sourcing to end-of-life disposal, with comparisons to materials commonly used in state-of-the-art devices. By placing sustainable materials at the core of the device concept, this work demonstrates a materials-driven design strategy for environmentally sustainable wearable sensors, offering a viable pathway toward next-generation sustainable wearable health technologies.

■ MATERIALS AND METHODS

Fabrication and Assembly of Sensing Devices

Chitosan sheets were prepared by dissolving chitosan oligosaccharide (6 g, COS; GU0761, Glentham Sciences) and chitosan (3 g, CS; GP8956, Glentham Sciences) in 1% acetic acid (200 mL, ≥9.8%, 33209, Merck Sigma) with glycerol (2 mL; ≥99%, G5516-1L, Merck Sigma) and citric acid (0.8 g; C1909-500G, Merck Sigma), followed by stirring, casting onto paper-covered Petri dishes, and drying for 3 days. LIG electrodes were patterned using a CO_2 laser cutter (90 W, xTool-P3, XLion Systems) and passivated with thin chitosan layers, except for total ionic strength sensor (TISS) sensing areas. Microfluidic layers were laser-cut from compostable PLA/natural rubber adhesive tape and laminated using a chitosan-coated protective adhesive layer. Before assembly, TISS electrodes were rinsed and dried, after which all layers were aligned, laminated onto the paper/chitosan/LIG substrates, and cut to the final device dimensions. See details in Supporting Information, Note S1.

LIG Electrode Characterization

XPS analysis was performed using a Thermo Fisher Nexsa system with Al Kα radiation, collecting survey and high-resolution spectra of C 1s, N 1s, and O 1s regions, which were analyzed using Advantage 2.6 software. Electrochemical impedance measurements were conducted with an MF312 Impedance Analyzer over frequencies from 10 Hz to 1 MHz. TISS performance was evaluated using NaCl solutions (0–200 mM), while sweat-rate sensing was characterized in vitro using controlled flow rates (0.5–5 μL min^{-1}) through a microfluidic system. Data were analyzed in MATLAB. Details of additional characterization and robustness tests are provided in Supporting Information, Note S1.

On-Body Experiments

On-body studies were approved by Delft University of Technology (Ethics Application No. 6130) and involved healthy participants (24–31 years) performing stationary cycling exercises while heart rate was monitored. Sweat was collected for off-body TISS validation, and sweat-rate sensors were attached to the back using medical adhesive and connected to an impedance analyzer. Five participants completed six exercise sessions, with all experiments performed using the same sensing platform and protocol as the in vitro studies. See Supporting Information, Note S1 for details.

LCA Analysis

A cradle-to-grave LCA was conducted in accordance with ISO 14040/14044[19,20] to evaluate the environmental impacts of the biodegradable chitosan-based sweat sensor. The assessment compared (i) the proposed chitosan/LIG device with a conventional PDMS-based device containing metal electrodes and (ii) LIG and metal electrodes within the same chitosan-based device architecture to isolate electrode-specific effects. The system boundary included material production, fabrication, assembly, transport, and end-of-life treatment.

Three scenarios were modeled: the proposed biodegradable chitosan/LIG device (S1), a conventional PDMS device with metal electrodes (S2), and a chitosan-based device with metal electrodes (S3). Material and energy inventories were derived from device fabrication data and linked to ecoinvent v3.12 datasets. Manufacturing processes, transport, electricity use, and fabrication waste were included, while proxy datasets were applied where material-specific data were unavailable.

Environmental impacts were assessed using the EF 3.1 Midpoint method, with interpretation focused on climate change, freshwater ecotoxicity, fossil resource use, and material resource use. Comparative and process contribution analyses were performed to quantify the environmental benefits of the overall device redesign and the specific replacement of metal electrodes with LIG. Detailed assumptions and inventories are provided in the Supporting Information, Note S2 and Supporting Information, Document 2.

■ RESULTS AND DISCUSSION

Our sustainable wearable sweat-sensing skin patch features a simple modular design that includes: a chitosan/chitosan oligosaccharide layer on a paper substrate, engraved LIG electrodes, and a laser-cut compostable microfluidic layer based on a compostable adhesive tape to channel the sweat (Figure 1a). It measures approximately 2.4 × 3.8 cm with a thickness of 500 μm. All materials used for the sensor are considered biodegradable and/or compostable (Figure 1a), reflecting the central design objective of minimizing the environmental footprint of a single-use sensing platform throughout its life cycle.

Once applied onto the skin, sweat enters the patch through an inlet with an effective area of approximately 0.125 cm^2. It is directed into a microfluidic network that features an

Downloaded from pubs.acs.org/ascecg/article-pdf/14/40/18238/6858153/sc-2026-07506n.pdf by TU DELFT user on 27 October 2026

https://doi.org/10.1021/acssuschemeng.6c07506
ACS Sustain. Chem. Eng. 2026, 14, 18238−18247

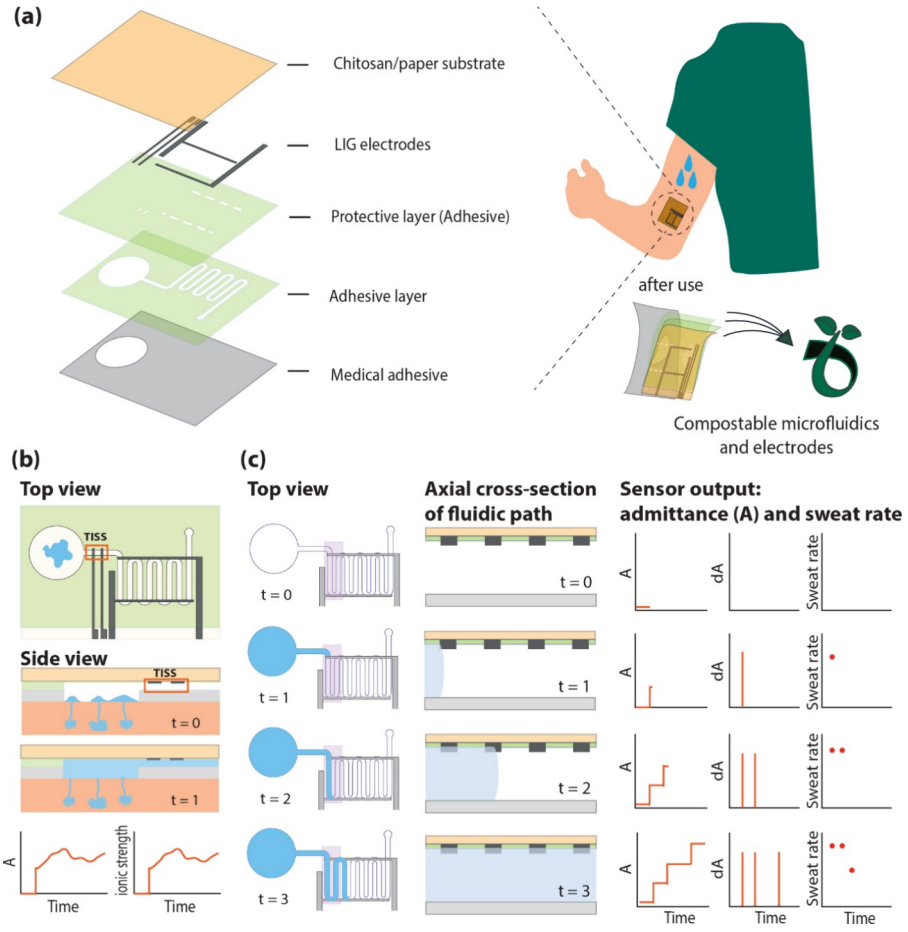


Figure 1. Design, fabrication, and operating principle of the sustainable-by-design wearable sweat patch. (a) Illustration of on-body sweat monitoring during physical activity including exploded schematic of the multilayer device architecture and a schematic highlighting the disposability and compostable nature of the microfluidic system and electrodes after use. (b) Top and side-view schematics illustrating sweat collection and filling of the inlet reservoir and microfluidic channel (in white), where the integrated impedimetric TISS (in gray) enables real-time ionic strength detection. (c) Conceptual diagram of the impedance-based sweat rate sensing mechanism. As sweat progresses through the microchannel, sequential contact with interdigitated electrodes induces stepwise increases in admittance ($1/|Z|$), which are used to quantify sweat rate by measuring the time intervals between admittance transitions. All schematics in this figure were created using Adobe Illustrator.

impedimetric total ionic strength sensor (TISS) composed of two electrodes (each 2 mm^2) placed in sequence. This setup allows for real-time detection of ionic strength as sweat accumulates and flows through the channel (Figure 1b). The fluid subsequently flows into a serpentine microchannel with a width of 800 μm and a height determined by the number of stacked adhesive layers (each approximately 66 μm thick), resulting in a configurable channel volume that can be adjusted from approximately 9 to 36 μL. Sweat transport through the microchannel occurs passively, driven by the natural negative pressure (i.e., suction) generated by sweat glands[21] and capillary forces. Downstream, two interdigitated LIG electrodes (400 μm finger width, 2.4 cm inter-electrode spacing) detect discrete changes in admittance ($1/|Z|$) as sweat progresses along the channel. Upon contact between the sweat front and the electrodes, the impedance decreases markedly due to increased ionic conductivity and capacitive coupling, yielding a corresponding increase in admittance. These admittance changes are recorded over time and used to quantify the sweat rate by monitoring the advancement of the sweat front through the microchannel with time (Figure 1c).

Fabrication and Characterization of Laser-Induced Graphene (LIG) Electrodes on Chitosan-Paper substrates

We first produced a flexible chitosan-paper substrate that is compatible with a one-step laser scribing process using a CO_2 infrared laser (λ = 10.6 μm) to form LIG electrodes (Figure 2a), eliminating the need for metallic inks or thin metal film electrodes. We optimized the composition of the chitosan film to create a flexible substrate that conforms to curved surfaces, such as the upper arm and forehead (Figure S1). To this end, films with varying chitosan (CS) and chitosan oligosaccharide (COS) ratios were prepared. While an increasing COS content yielded more conductive LIG structures (i.e., values as low as 0.50 ± 0.1 Ω/sq sheet resistance), COS-based films showed cracking during drying or bending of the films (Figure S1).

To address these issues, we incorporated glycerol as a plasticizer, which improved the film's flexibility and prevented cracking, even with higher COS contents. Additionally, we introduced citric acid crosslinking to reduce film swelling (Figure S2). For enhanced mechanical robustness and more reproducible sheet production, we used paper as a supporting

https://doi.org/10.1021/acssuschemeng.6c07506
ACS Sustain. Chem. Eng. 2026, 14, 18238−18247

Downloaded from pubs.acs.org/ascecg/article-pdf/14/40/18238/6858153/sc-2026-07506n.pdf by TU DELFT user on 27 October 2026

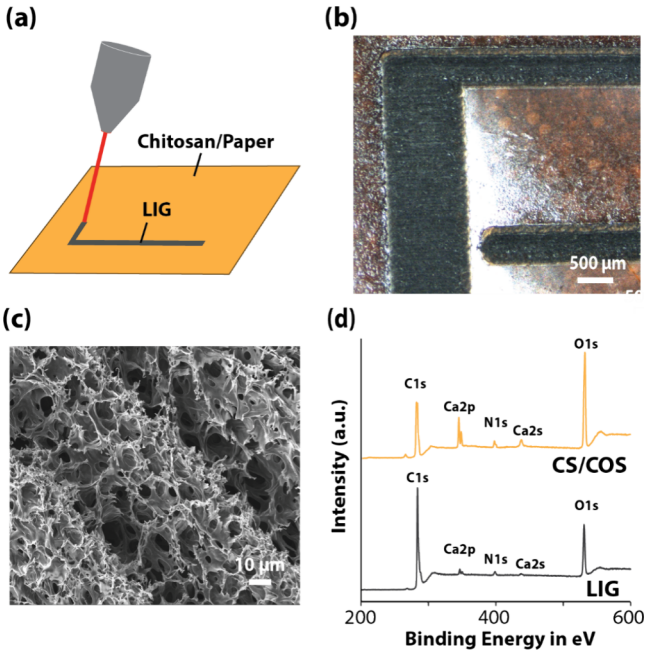


Figure 2. Fabrication and characterization of LIG on chitosan/paper substrates. (a) Schematic of the one-step CO_2 laser scribing process to convert the chitosan-paper surface into LIG (created using Adobe Illustrator). (b) Optical image of a representative LIG electrode showing well-defined and clean edges (scale bar: 500 μm). (c) SEM image revealing a highly porous and interconnected carbon network formed after laser conversion (scale bar: 10 μm). (d) XPS spectra of the paper/chitosan substrate without (yellow) and with LIG structures (gray), indicating increased carbon content and reduced oxygen content after LIG formation.

substrate. Once a flat and robust sheet could be reliably produced, we proceeded with LIG fabrication varying the laser scribing parameters (i.e., laser power and laser speed) to achieve full conversion to LIG (Figure S3). Based on this combined optimization of film composition and scribing conditions, a CS:COS ratio of 1:2 was selected, yielding robust films with engraved LIG structures exhibiting a sheet resistance of approximately 16.5 ± 1.0 Ω/sq.

The optimized LIG patterns on the paper/chitosan substrate exhibited clean, well-defined edges (Figure 2b), and scanning electron microscopy (SEM) analysis revealed a characteristic porous and interconnected carbon network in the fully converted LIG samples (Figure 2c). We further analyzed the paper/chitosan/LIG structures using X-ray photoelectron spectroscopy (XPS). Compared to the paper/chitosan substrate without LIG, the LIG samples exhibited a clear increase in carbon peak intensity, corresponding to an increase in overall carbon content from 62.5 ± 4.3% to 77.5 ± 1.1% (Figure 2d). This was accompanied by an increase in graphitic (sp^2) carbon and a reduction in oxygen-containing functional groups. The oxygen content decreased from 29.1 ± 2.9% to 16.9 ± 1.5%, nearly halving after laser conversion, further confirming the successful carbonization and formation of LIG structures on the paper/chitosan substrate (Figure S4).

To evaluate surface wettability, we measured the contact angle, revealing the highly hydrophilic nature of the paper/chitosan/LIG surface ($\theta < 10°$), which adsorbed water immediately upon deposition (Figure S5). Due to this high hydrophilicity, a passivation layer was required to prevent liquid spreading across the electrodes and potential leakage when incorporated into a microfluidic device. The application of a thin chitosan coating effectively confined the liquid to a defined electrode area ($\theta = 50° \pm 2°$) while still allowing sufficient wetting for impedimetric sweat rate sensing (Figure S5).

Following optimization of the sustainable electrodes, a compostable microfluidic unit composed of laser-cut layers of compostable adhesive was integrated with the LIG electrodes. This laser-cut microfluidics approach, based on adhesive or foil layers, provides a simple, eco-conscious, and low-cost alternative to state-of-the-art PDMS-based microfluidic systems. Optimization of the laser-cutting process minimized deformation of the cut edges in the adhesive (Figure S6).

Sweat Rate Sensor Operation and Characterization

We next evaluated whether these sustainable-by-design material choices could deliver the functional performance required for practical sweat monitoring applications. The impedance-based sensing performance of the sweat patch was systematically evaluated in vitro. The TISS was tested with NaCl solutions of varying concentrations, measuring the impedance response of the LIG electrode pair across a broad frequency range (Figure 3a). The impedance signal exhibited a strong dependence on ionic strength, decreasing with higher ionic strength due to increased charge-carrier density. The sensitivity was highest within the frequency range of 1 to 100 kHz (Figure S7), leading to the selection of 100 kHz for further testing. When exposed to a sequence of increasing and decreasing concentrations of NaCl, we observed reproducible, concentration-dependent changes in admittance (Figure 3b). The extracted admittance values displayed a strong linear correlation with the logarithm of NaCl concentration, yielding a sensitivity of 70 μS per log(mM) NaCl (Figure 3c). The limit of detection (LOD) was determined to be 1 mM, with a linear dynamic range for the TISS extending from 1 mM to 200 mM (Figure S7 and Figure 3c) covering the physiologically relevant ionic strength expected in sweat.[22] However, we observed batch-to-batch variation, indicating that pre-use calibration is necessary for consistent quantitative evaluation across devices.

When tested for selectivity, the sensor responded consistently to changes in total ionic strength from both mono- and divalent ions (K^+, Mg^{2+}, Ca^{2+}; Figure S7). Presence of glucose or proteins had negligible effect, consistent with their minimal contribution to bulk ionic strength, while lactic acid increased the readout due to its partial dissociation into lactate and H^+ (Figure S7).

The sensor's output was unaffected by flow rate (1–50 μL min^{-1}, <1 μS variation) and showed stable baselines across temperatures, despite an expected temperature-dependent decrease in impedance (Figure S8), confirming its robustness for real-time ionic strength monitoring over the 30-min in vitro testing period. At longer time scales however, a baseline drift of up to 15 μS per hour was observed, which is attributed to swelling of the chitosan substrate (Figure S8).

We further tested the TISS at three curvatures (radii of 2.5, 4, and 6 cm; Figure S8). Admittance remained unaffected at radii of 6 cm or higher, while at 2.5 cm, outward and inward bending altered admittance by up to 8% ± 1% and 10% ± 6%, respectively, with irreversible microcracking observed after multiple bending cycles (10+, Figure S8). Considering this mechanical

Downloaded from pubs.acs.org/ascecg/article-pdf/14/40/18238/6858153/sc-2026-07506n.pdf by TU DELFT user on 27 October 2026

https://doi.org/10.1021/acssuschemeng.6c07506
ACS Sustain. Chem. Eng. 2026, 14, 18238–18247

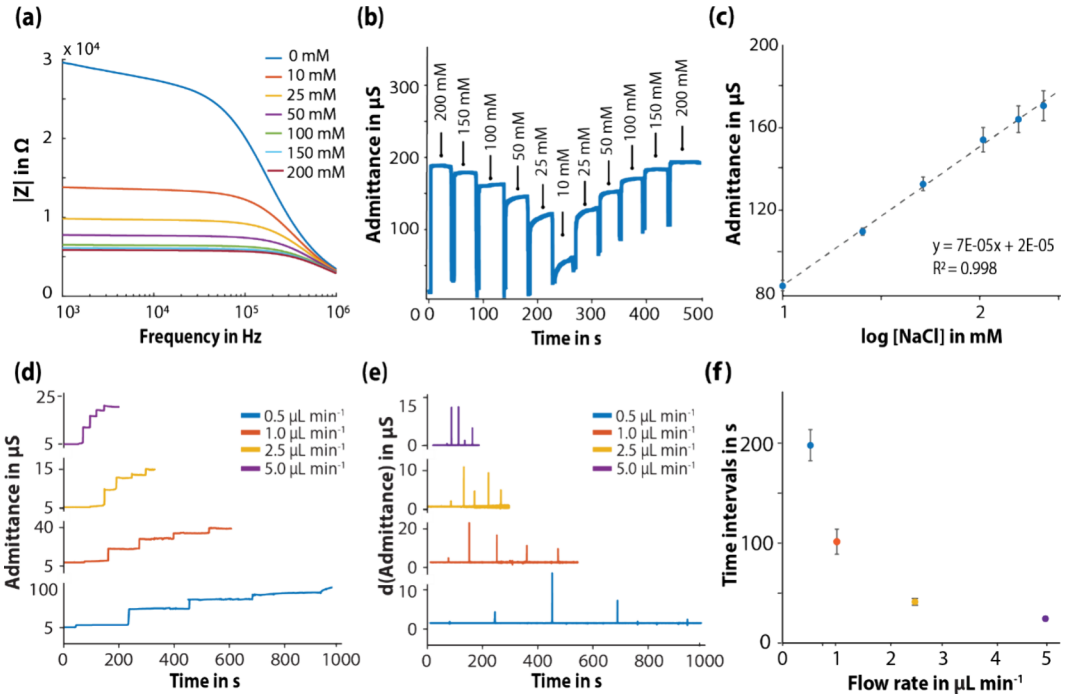


Figure 3. In vitro characterization of ionic sensing and sweat-rate detection. (a) Frequency-dependent impedance ($|Z|$) of the TISS exposed to NaCl solutions from 0 to 200 mM, demonstrating decreasing impedance with increasing ionic strength. (b) Representative admittance response over time at 100 kHz upon sequential exposure to NaCl solutions of varying concentrations, showing stepwise and reversible signal changes. (c) Calibration curve of admittance vs the logarithm of NaCl concentration at 100 kHz, indicating a linear relationship ($R^2 = 0.998$). (d) Representative admittance response of the sweat-rate sensor to a constant NaCl concentration (100 mM) at different flow rates, illustrating stepwise increases corresponding to fluid progression through the channel. (e) Differential admittance signals d(Admittance/dt), where each spike corresponds to a discrete filling event; spike frequency increases with flow rate. (f) Extracted time intervals between successive spikes as a function of flow rate, demonstrating an inverse relationship and enabling quantitative flow-rate determination.

limitation, these results indicate that flatter, less dynamically strained (i.e., radii 6 cm or higher) wearing sites support stable performance.

Next, we characterized the sweat rate sensing unit using a configuration with two fingers to ensure robust signals for our proof-of-concept study. To validate the accuracy of the flow rate measurements, the sensor's output was benchmarked against reference flow rates generated by a commercial syringe pump. The response of the sweat rate sensor to controlled flow inputs of 100 mM NaCl solution is shown in Figure 3d. At higher flow rates, the frequency of admittance jumps increased proportionally over time. By identifying these events-defined as sharp rises in the time derivative of the admittance signal-the flow rate through the microchannel was determined (Figure 3e). The time intervals between admittance jumps correlated as expected with the syringe pump flow rate (Figure 3f). The sweat rate sensor's current resolution, based on in vitro calibration, is limited to approximately 6% of the set flow rate, which primarily affects reliability at higher flow rates. An increase in the resolution of the sweat rate sensing unit can be achieved by optimizing the number of electrode fingers (Figure S9), as demonstrated by a previously developed impedimetric sweat rate sensor.[7] The versatility of the system in accommodating different sweat volumes was demonstrated through extended microfluidic designs, achieved by increasing the number of serpentines or adopting a multilayer configuration to enhance sweat collection volume (Figure S9). The response time scaled linearly with channel height, reaching a maximum sweat volume of approximately 36 µL, which would allow for more than 2 h of monitoring in moderate exercise scenarios with sweat rates between 0.1 to 1 µL min^{-1} cm^{-2}.[23]

While both the TISS and sweat-rate sensing units are subject to mechanical strain, temperature fluctuations, and hydration-induced swelling, their distinct sensing principles make them differentially sensitive to these effects. The TISS relies on stable, absolute impedance values, such that baseline shifts arising from bending, temperature, or substrate swelling directly propagate into measurement error (Figures S7 and S8). Sweat-rate sensing, by contrast, depends on the relative timing of discrete admittance changes rather than their absolute magnitude; it is inherently more tolerant of slowly evolving or globally applied baseline shifts. This distinction accounts for the robustness of on-body sweat-rate monitoring; the same set of factors currently confines the TISS to more controlled, off-body analysis.

Although this represents a limitation for the present TISS design, it simultaneously highlights opportunities for further improvements in future studies: temperature compensation strategies and optimized chitosan crosslinking are expected to stabilize the substrate, thereby enhancing reliability and extending the TISS toward full on-body operation in future iterations.

Functionality of the Sensor Patch in a Physical Exercise Scenario

The performance of the sustainable sweat-sensing patch was then evaluated under physiologically relevant conditions using a controlled stationary cycling set-up (Figure 4a).

Downloaded from pubs.acs.org/ascecg/article-pdf/14/40/18238/6858153/sc-2026-07506n.pdf by TU DELFT user on 27 October 2026

https://doi.org/10.1021/acssuschemeng.6c07506
ACS Sustain. Chem. Eng. 2026, 14, 18238−18247

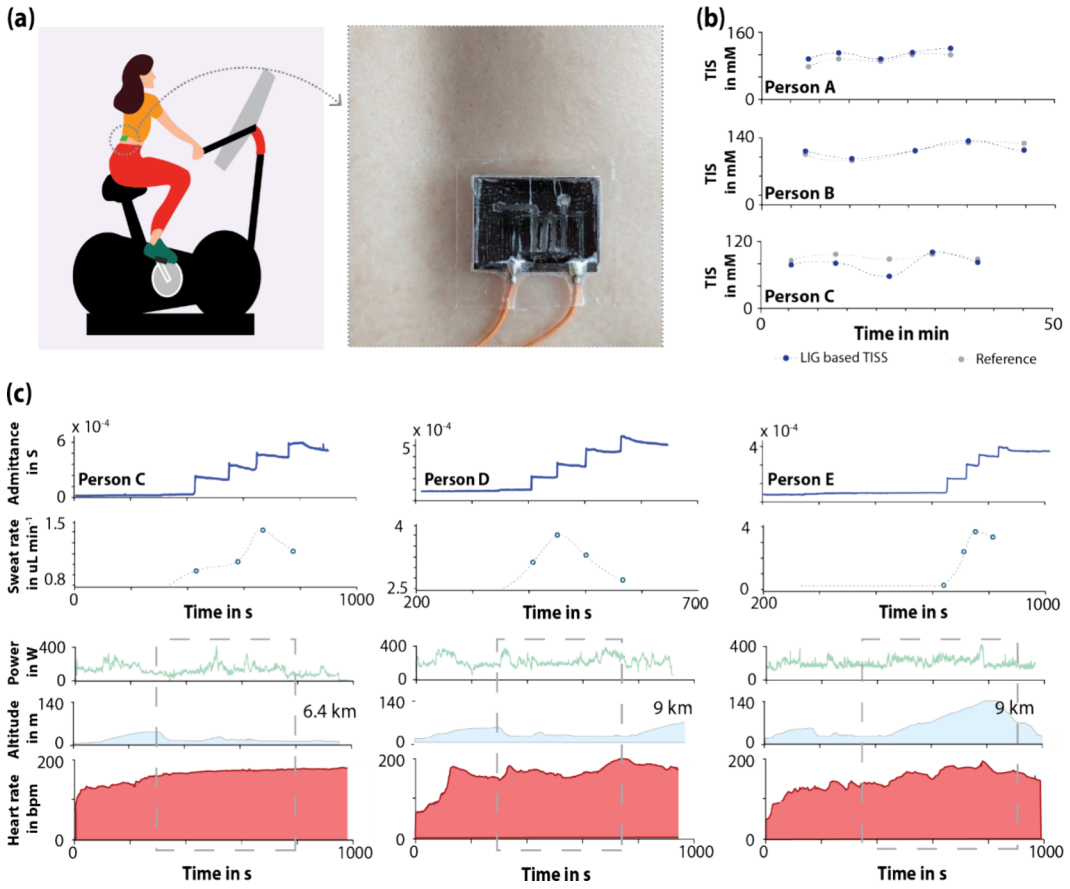


Figure 4. Real-time monitoring of sweat ionic strength and physiological parameters during exercise. (a) Schematic illustration of a participant performing cycling exercise while wearing the wearable sweat sensor and photograph of the patch placed on the lower back. Schematic was created using Adobe Illustrator. (b) Temporal profiles of total ionic strength (TIS) measured in mM for three participants (A–C) over 45 min, demonstrating the sensor's ability to capture dynamic changes in sweat composition. (c) Detailed high-resolution recordings from three additional participants (C–E) showing: (top) sweat admittance in μS, (second row) sweat rate in μL/min, (third row) power in W reflecting the participant's cycling power output (i.e., exercise intensity), (fourth row) altitude profile in meters, and (bottom) heart rate in bpm over time illustrating sweat ionic response, physiological exertion, and cardiovascular load during cycling.

Sweat rate sensing was evaluated on-body using microfluidic patches placed on the lower back (Figure 4c) with an optically transparent control patch positioned nearby to visually monitor fluid progression (Figure S10). Across all participants, the admittance signals exhibited distinct stepwise increases corresponding to the advancement of sweat through the microfluidic channel (Figure 4c), enabling the successful extraction of sweat rates in real time. The sensor captured clear and dynamic changes in sweating behavior that differed between each individual, showing personalized sweat rate profiles. For example, Participant E showed a delayed onset with an initially low sweat rate of approximately 0.3 μL min^{-1}, followed by a marked increase at higher exercise intensity, correlating with an elevated heart rate (Figure 4c, right column). These results demonstrate that the system enables personalized analysis of ionic strength and on-body monitoring of sweat rate dynamics during exercise. Although the current sample size of $n = 3$ remains limited and further validation with complementary methods is necessary, the data presented offer a proof of concept for the use of fully biodegradable and compostable materials, while providing physiologically relevant data.

To assess the clinical relevance of TISS, sweat samples of human subject were collected approximately every 7 min over a 35–50 min exercise period from a 2 × 2 cm^2 area on the lower back (Figure S10). Due to the swelling behavior of chitosan that currently limits stable on-body deployment, the collected samples were analyzed off-body using the fabricated sensor and benchmarked against a gold electrode-based TISS. The results demonstrated strong agreement, with only a small bias (−1.69 mM), while the wider limits of agreement (+26 mM and −29 mM) suggest that different referencing is necessary, as the expected deviation of the LIG-based TISS would be the overestimation of the total ionic strength, whereas the gold electrodes occasionally recorded higher trends. Despite the wider limits of agreement currently limiting use for absolute quantification, the developed TISS reliably captured temporal changes in ionic strength, consistently reproducing overall trends. Future work targeting chitosan matrix stability is thus expected to substantially narrow the limits of agreement, moving the TISS from a reliable trend-tracking platform toward one capable of clinical-grade absolute quantification (Supporting Information, Note S3).

LCA Results

The environmental impact of the proposed sweat patch (S1) was quantified at two levels: the full device and the electrode.

Downloaded from pubs.acs.org/ascecg/article-pdf/14/40/18238/6858153/sc-2026-07506n.pdf by TU DELFT user on 27 October 2026

https://doi.org/10.1021/acssuschemeng.6c07506
ACS Sustain. Chem. Eng. 2026, 14, 18238−18247

First, our sustainable-by-design device was compared with a conventional PDMS–metal device of equivalent functionality (see Materials and Methods, S2). Then, the role of electrode material was isolated through a sensitivity analysis, where LIG electrodes were replaced with conventional metals while maintaining the chitosan-based architecture (S3). This two-level comparison allows the environmental benefits of the overall device redesign to be distinguished from those specifically attributable to electrode substitution.

Figure 5a shows that S1 consistently outperforms S2 across all EF 3.1 midpoint categories. The largest improvement occurs in material resource use (metals and minerals), reduced by 98.1%. As shown in Figure 5b, S2 is heavily dominated by the gold supply chain, with unrefined gold production contributing 42.6% and gold–silver mining and refining an additional 20.8%. In contrast, S1 largely avoids dedicated metal inputs, with only minor contributions from background processes. This confirms that LIG electrodes significantly reduce dependence on extractive metal supply chains.

Freshwater ecotoxicity shows a similarly pronounced improvement with our device, with S2 (3.525 CTUe) exceeding S1 (0.113 CTUe) by more than an order of magnitude. This burden in S2 arises mainly from PDMS production (1.690 CTUe, or 47.9% of the total freshwater ecotoxicity result) and gold mining residues (1.044 CTUe), whereas S1 exhibits only minimal contributions from upstream processes (<0.008 CTUe each). These results indicate that eliminating both PDMS and gold electrodes is key to reducing ecotoxicity.

S1 also lowers climate change impact by 53.0% (Figure 5a). In S2, emissions are dominated by cleanroom-assisted electrode fabrication (31.5%), metal thin-film production (25.9%), assembly energy (18.7%), and PDMS production (18.6%). In contrast, S1's impact is primarily driven by electricity use during fabrication, particularly for laser processing, reflecting the Dutch energy mix (Figure 5b).

A similar trend is observed for non-renewable energy use: S2 (0.836 MJ) has roughly double the impact of S1 (0.406 MJ), due to fossil-intensive PDMS production, cleanroom processes, and metal fabrication. By avoiding these steps, S1 substantially reduces fossil energy demand.

Additional improvements include reductions in water consumption (−49.3%), land use (−51.7%), carcinogenic toxicity (−87.1%), and non-carcinogenic toxicity (−76.4%). Other categories, such as acidification, eutrophication, particulate matter formation, and photochemical oxidant formation, also show consistent decreases (Figure 5a and Table S1). Interestingly, although S1 includes biodegradable components, end-of-life

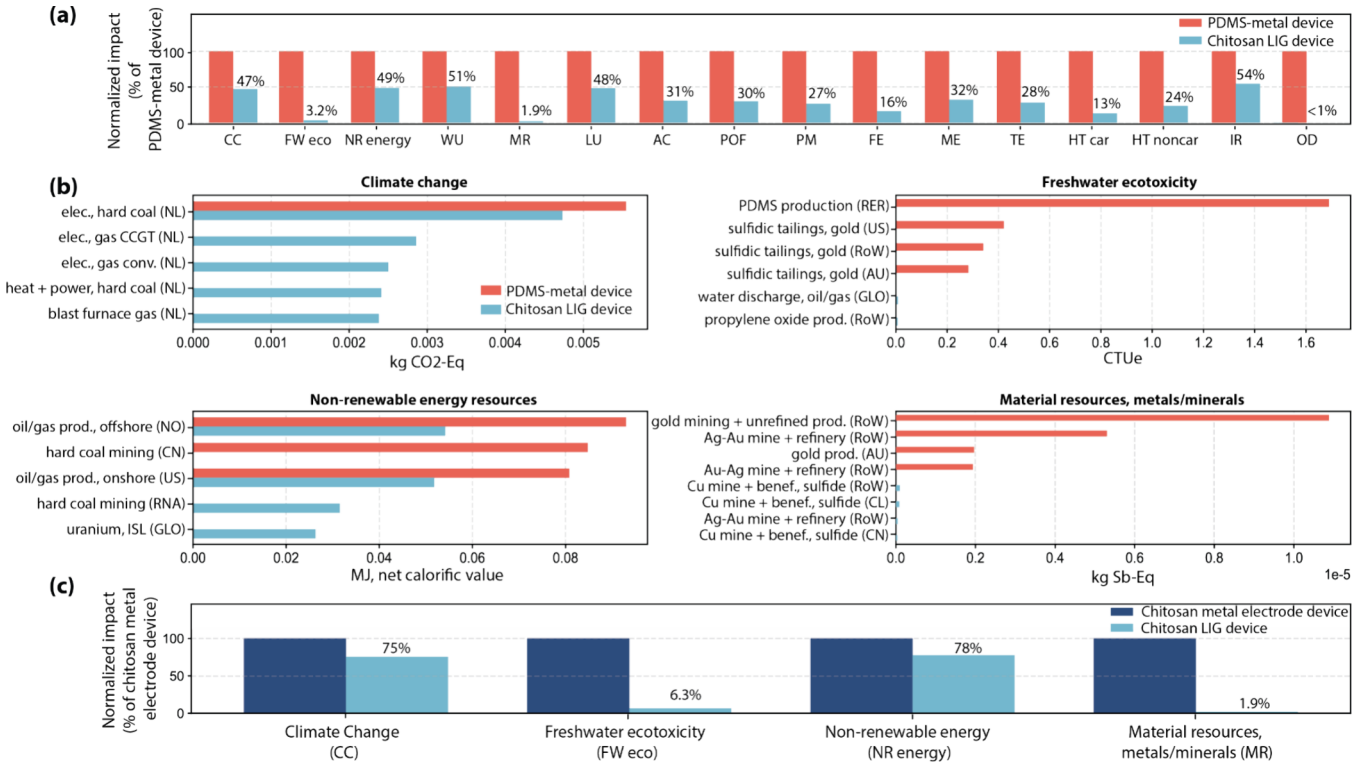


Figure 5. Life cycle assessment quantifies the environmental impact of the developed chitosan LIG sweat sensor and comparison with reference device scenarios. Scenario 1 (S1) represents the developed chitosan LIG device, Scenario 2 (S2) represents a conventional PDMS metal device, and Scenario 3 (S3) represents the chitosan metal electrode device. (a) Normalized cradle-to-grave impacts across EF 3.1 midpoint categories for S1 and S2. Results are expressed as a percentage of S2 within each impact category. Values above the S1 bars indicate the impact of S1 as a percentage of S2. (b) Process contribution analysis for four representative impact categories in the S1 and S2 comparison, namely climate change, freshwater ecotoxicity, nonrenewable energy resources, and material resources, metals and minerals. (c) Electrode sensitivity comparison between S1 and S3 within the same chitosan-based device platform. Results are expressed as a percentage of S3 within each impact category. Values above the S1 bars indicate the impact of S1 as a percentage of S3. Category abbreviations used: CC, climate change; FW eco, freshwater ecotoxicity; NR energy, non renewable energy resources; WU, water use; MR, material resources, metals and minerals; LU, land use; AC, acidification; POF, photochemical oxidant formation; PM, particulate matter formation; FE, freshwater eutrophication; ME, marine eutrophication; TE, terrestrial eutrophication; HT car, human toxicity, carcinogenic; HT noncar, human toxicity, non carcinogenic; IR, ionizing radiation; OD, ozone depletion.

Downloaded from pubs.acs.org/ascecg/article-pdf/14/40/18238/6858153/sc-2026-07506n.pdf by TU DELFT user on 27 October 2026

https://doi.org/10.1021/acssuschemeng.6c07506
ACS Sustain. Chem. Eng. 2026, 14, 18238−18247

contributes only marginally to total impacts. For example, composting provides a small climate credit (−0.61%) due to the low material mass and limited avoided burdens. Nonetheless, it offers a more sustainable disposal pathway for single-use wearable devices.

These results demonstrate that the benefits of S1 extend beyond a single material substitution. Instead, they arise from avoiding the combined burdens of PDMS microfluidics, metal electrodes, and cleanroom fabrication. The largest gains, particularly in ecotoxicity and metal resource use, are driven by eliminating gold-based supply chains. Reductions in climate change, energy use, and other categories reflect lower environmental impacts across both material production and fabrication stages.

To isolate the effect of electrode selection from the broader device architecture, an electrode sensitivity analysis was performed comparing S1 and S3 (Figure 5c). In this comparison, both devices share the same chitosan-based structure but differ in electrode type. The results show that S1 has lower impacts than S3 across all four selected categories. The influence of electrode selection is most pronounced in freshwater ecotoxicity and material resource use. Freshwater ecotoxicity drops sharply from 1.781 CTUe in S3 to 0.113 CTUe in S1, corresponding to a 93.7% reduction. Similarly, material resource use (metals and minerals) decreases by 98.1%. Other improvements include: climate change decreases by 24.7%, non-renewable energy resource by 22.4%.

To further assess the sensitivity of the S3 results to the assumed metal-electrode dimensions, we performed a sensitivity analysis (Supporting Information, Notes S2 and S4) evaluating five Au/Cr-coated-area scenarios (2 to 0.08 cm^2) to isolate the effective gold-coated areas as a factor and preserve an unbiased comparative assessment. Climate change and non-renewable energy resources were relatively insensitive to Au/Cr loading (reductions plateauing around 47–49%), indicating 51% are associated with non-metal components and processes. In contrast, freshwater ecotoxicity and material resources were highly sensitive to gold content (reductions up to ∼91–95%), reflecting the significant resource-depletion and upstream emission burdens associated with precious-metal production.

The above results indicate that the primary environmental advantage of LIG electrodes arises from avoiding metal thin-film supply chains, particularly those associated with gold extraction and refining. Overall, the findings confirm that the improved performance of S1 stems from two key design choices: the biodegradable chitosan-based platform in replacement of PDMS and the use of a non-metal conductive strategy based on LIG.

CONCLUSIONS

We developed a sustainable-by-design, low-cost, and flexible wearable sweat-sensing patch capable of real-time monitoring of both sweat ionic strength and sweat rate during exercise. The platform replaces conventional non-degradable polymers and metal-based electrodes with biodegradable and compostable materials, using LIG electrodes on a flexible chitosan-paper substrate integrated into a compostable microfluidic system. This design simplifies device assembly and enables customizable adjustments through its modular architecture.

The platform successfully showed sensing performance for wearable sweat monitoring, with reliable ionic strength and sweat-rate measurements across physiological ranges. On-body testing in a physical exercise scenario demonstrated the ability to monitor sweat rate directly on skin, allowing for capturing temporal changes in dynamic sweat-rate profiles of the participants. We also demonstrated the device's ability to quantify total ionic strength changes in real sweat collected from the back of three different subjects. While further clinical validation with improved referencing methods is needed, these results demonstrate the potential of fully biodegradable sweat-sensing platforms for sustainable, continuous, and non-invasive monitoring of human physiology in real-world applications.

Life cycle assessment showed that the developed chitosan LIG device outperforms the conventional PDMS metal reference device across all assessed EF 3.1 impact categories. The reduction was clear for climate change, non-renewable energy resource use, water use, and land use, and was especially strong for freshwater ecotoxicity and material resources, metals and minerals. These improvements arise from the combined material and fabrication strategy, including elimination of metal electrodes and cleanroom processing. Electrode sensitivity analysis further confirmed the key contribution of LIG in reducing environmental impacts.

This work demonstrates that sustainable material and fabrication choices can be effectively integrated into wearable chemical sensors without substantially compromising performance. The current prototype's limitations relative to state-of-the-art systems stem largely from substrate hydrophilicity and fabrication reproducibility, reflecting an earlier stage of development rather than an inherent drawback of biodegradable platforms. Future optimization of substrate crosslinking, fabrication standardization, and laser-scribing is expected to narrow this gap through batch- or device-level calibration, while preserving the environmental benefits demonstrated by this study's LCA. With the rapidly growing demand for personal health-monitoring sensors, sustainability should become an essential design criterion in the development of next-generation wearable technologies, and this work demonstrates a promising and practical pathway toward achieving high-performance, environmentally responsible sensing platforms.

ASSOCIATED CONTENT

Supporting Information

The Supporting Information is available free of charge at https://pubs.acs.org/doi/10.1021/acssuschemeng.6c07506.

Detailed methods and materials; fabrication and characterization of CS:COS substrates and LIG electrodes; swelling behavior and mechanical properties of crosslinked films; additional SEM and XPS analysis of substrates and LIG; contact angle measurements; laser-cutting calibration of adhesive layers; frequency-dependent response and temporal stability of the TISS; TISS performance with divalent ions, glucose, lactic acid, BSA, varying flow rate, and temperature; design optimization of the sweat-rate sensor via microfluidic and electrode architecture; additional on-body validation data; passivation and microfluidic layer designs; and LCA setup, system boundaries, and process flow (PDF)

Life cycle inventory of LCA (PDF)

AUTHOR INFORMATION

Corresponding Author

Alina Y. Rwei – *Department of Chemical Engineering, TU Delft, Van de Maasweg 9, Delft 2629 HZ, The Netherlands;*

Downloaded from pubs.acs.org/ascecg/article-pdf/14/40/18238/6858153/sc-2026-07506n.pdf by TU DELFT user on 27 October 2026

https://doi.org/10.1021/acssuschemeng.6c07506
ACS Sustain. Chem. Eng. 2026, 14, 18238−18247

orcid.org/0000-0001-6080-579X;
Email: a.y.rwei@tudelft.nl

Authors

Lena Fasching – *Department of Chemical Engineering, TU Delft, Van de Maasweg 9, Delft 2629 HZ, The Netherlands*

Justin Z. Lian – *Institute of Environmental Science – Industrial Ecology, Leiden University, Van Steenisgebouw, Einsteinweg 2, Leiden 2333 CC, The Netherlands; Copernicus Institute of Sustainable Development, Utrecht University, Vening Meinesz Building A, Princetonlaan 8a, Utrecht 3584 CB, The Netherlands*

Stefano Cucurachi – *Institute of Environmental Science – Industrial Ecology, Leiden University, Van Steenisgebouw, Einsteinweg 2, Leiden 2333 CC, The Netherlands*

Complete contact information is available at: https://pubs.acs.org/doi/10.1021/acssuschemeng.6c07506

Author Contributions

°L.F. and J.Z.L. contributed equally to this work. Conceptualization: L.F., J.Z.L., and A.Y.R.; methodology: L.F. and J.Z.L.; data acquisition and analysis: L.F. and J.Z.L.; writing-original draft: L.F. and J.Z.L.; writing, review and editing: L.F., J.Z.L., S.C., and A.Y.R.

Funding

This study was funded by Convergence Health and Technology, an alliance between TU Delft, Erasmus Medical Center, and Erasmus University Rotterdam. The collaborative project is co-funded through the use of PPS subsidy awarded by Health~Holland, Top Sector Life Sciences & Health, in collaboration with the Worktech Program Group, to stimulate public-private partnerships.

Notes

The authors declare no competing financial interest.

■ ACKNOWLEDGMENTS

We would like to thank all participants for their hard work and dedication during the exercise. A special thanks goes to M. F. Theissen for providing the stationary bicycle setup, and to E. D. Özerk for her help with setting up the on-body study test set-up. We also wish to express our gratitude to 3M Netherlands and Monta Germany for supplying us with samples of the medical and compostable adhesives.

■ REFERENCES

(1) Min, J.; Tu, J.; Xu, C.; Lukas, H.; Shin, S.; Yang, Y.; Solomon, S. A.; Mukasa, D.; Gao, W. Skin-Interfaced Wearable Sweat Sensors for Precision Medicine. *Chem. Rev.* **2023**, *123* (8), 5049–5138.

(2) Ghaffari, R.; Yang, D. S.; Kim, J.; Mansour, A.; Wright, J. A.; Model, J. B.; Wright, D. E.; Rogers, J. A.; Ray, T. R. State of Sweat: Emerging Wearable Systems for Real-Time, Noninvasive Sweat Sensing and Analytics. *ACS Sens.* **2021**, *6* (8), 2787–2801.

(3) Yang, C.; Wang, B.; Wan, J.; Kamath, A.; You, F.; Tian, B. Quantifying the Global Eco-Footprint of Wearable Healthcare Electronics. *Nature* **2026**, *649* (8095), 73–82.

(4) Ates, H. C.; Nguyen, P. Q.; Gonzalez-Macia, L.; Morales-Narváez, E.; Güder, F.; Collins, J. J.; Dincer, C. End-to-End Design of Wearable Sensors. *Nat. Rev. Mater.* **2022**, *7* (11), 887–907.

(5) Yuan, Z.; Hou, L.; Bariya, M.; Nyein, H. Y. Y.; Tai, L.-C.; Ji, W.; Li, L.; Javey, A. A Multi-Modal Sweat Sensing Patch for Cross-Verification of Sweat Rate, Total Ionic Charge, and Na^+ Concentration. *Lab Chip* **2019**, *19* (19), 3179–3189.

(6) Nyein, H. Y. Y.; Tai, L.-C.; Ngo, Q. P.; Chao, M.; Zhang, G. B.; Gao, W.; Bariya, M.; Bullock, J.; Kim, H.; Fahad, H. M.; Javey, A. A Wearable Microfluidic Sensing Patch for Dynamic Sweat Secretion Analysis. *ACS Sens.* **2018**, *3* (5), 944–952.

(7) Lian, J. Z.; Siebler, F.; Steubing, B. R. P.; Jesorka, A.; Barbarossa, V.; Wang, R.; Leo, K.; Sen, I.; Cucurachi, S. Quantifying the Present and Future Environmental Sustainability of Cleanrooms. *Cell Rep. Sustain.* **2024**, *1* (9), No. 100219.

(8) Williams, A.; Aguilar, M. R.; Pattiya Arachchillage, K. G. G.; Chandra, S.; Rangan, S.; Ghosal Gupta, S.; Artes Vivancos, J. M. Biosensors for Public Health and Environmental Monitoring: The Case for Sustainable Biosensing. *ACS Sustain. Chem. Eng.* **2024**, *12* (28), 10296–10312.

(9) Tjokro, K. J.; Barbarossa, V.; Cucurachi, S.; Rwei, A.; Lian, J. Assessing the Environmental Impacts of Microfluidic Devices for Glucose Detection. *ACS Sustain. Chem. Eng.* **2025**, *13* (25), 9500–9509.

(10) Bauer, M.; Wunderlich, L.; Weinzierl, F.; Lei, Y.; Duerkop, A.; Alshareef, H. N.; Baeumner, A. J. Electrochemical Multi-Analyte Point-of-Care Perspiration Sensors Using on-Chip Three-Dimensional Graphene Electrodes. *Anal. Bioanal. Chem.* **2021**, *413* (3), 763–777.

(11) Wang, X.; Zeng, M.; Torrens, M.; Niu, P.; Fernández Sánchez, C.; Gich, M.; Roig, A. Eco-Friendly Conformal and Self-Adhesive Electrochemical Sensors for Sweat Monitoring. *ACS Appl. Mater. Interfaces* **2025**, *17* (39), 54411–54422.

(12) Garland, N. T.; Schmieder, J.; Johnson, Z. T.; Hjort, R. G.; Chen, B.; Andersen, C.; Sanborn, D.; Kjeldgaard, G.; Pola, C. C.; Li, J.; Gomes, C.; Smith, E. A.; Angus, H.; Meyer, J.; Claussen, J. C. Wearable Flexible Perspiration Biosensors Using Laser-Induced Graphene and Polymeric Tape Microfluidics. *ACS Appl. Mater. Interfaces* **2023**, *15* (32), 38201–38213.

(13) Moon, H.; Ryu, B. Review of Laser-Induced Graphene (LIG) Produced on Eco-Friendly Substrates. *Int. J. Precis. Eng. Manuf.-Green Technol.* **2024**, *11* (4), 1279–1294.

(14) Hamidi, H.; Levieux, J.; Larrigy, C.; Russo, A.; Vaughan, E.; Murray, R.; Quinn, A. J.; Iacopino, D. Laser Induced Graphene (LIG) Biosensors Derived from Chitosan: Towards Sustainable and Green Electronics. *Biosens. Bioelectron. X* **2023**, *15*, No. 100403.

(15) Steksova, Y.; Bressi, A. C.; Galliani, M.; Marino, A.; Ciofani, G.; Machado-Charry, E.; Bernal, H. G.; Francini, A.; Sebastiani, L.; Greco, F. Laser-Induced Graphene from Waste Almond Shells *Adv. Funct. Mater.* **2025**, No. e07462.

(16) Ghavipanjeh, A.; Sadeghzadeh, S.; Naghib, S. M.; Dashtian, K. Flexible Laser-Induced Graphene Microelectrochemical Sensor on Sustainable Cellulosic Paper Substrate for Sensitive Detection of Uric Acid and Tyrosine in Sweat. *Langmuir* **2026**, *42* (9), 7027–7038.

(17) Rabost-Garcia, G.; Sanchez, D.; Nacher-Castellet, V.; Fajardo, A.; Ymbern, O.; Muñoz-Pascual, X.; Alvarez, A.; Punter-Villagrasa, J.; Casals-Terré, J.; Heredia, R.; Espinoza, F.; Moreno-Simonet, L.; Cosio, P. L. L.; Cadefau, J. A.; Marwede, M.; Ongaro, A. E. Early-Stage Life Cycle Assessment for Sustainable Design of Wearable Microfluidic Sweat Sensor: Continuous Dehydration Monitoring. *Front. Lab Chip Technol.* **2025**, *4*, No. 1688689.

(18) Cai, J.; Sun, M.; Wang, J.; Xiao, Z.; Bai, J.; Ma, C.-B.; Bo, X.; Ding, S.; Zhou, M. Woodtronics for Sustainable and Flexible Epidermal Sweat Sensing. *Device* **2026**, *4* (7), No. 101179.

(19) ISOISO 14040: 2006. https://www.iso.org/standard/37456.html (accessed 2026-04-20).

(20) ISOISO 14044:2006. https://www.iso.org/standard/38498.html (accessed 2026-04-20).

(21) Choi, J.; Xue, Y.; Xia, W.; Ray, T. R.; Reeder, J. T.; Bandodkar, A. J.; Kang, D.; Xu, S.; Huang, Y.; Rogers, J. A. Soft, Skin-Mounted Microfluidic Systems for Measuring Secretory Fluidic Pressures

Downloaded from pubs.acs.org/ascecg/article-pdf/14/40/18238/6858153/sc-2026-07506n.pdf by TU DELFT user on 27 October 2026

Generated at the Surface of the Skin by Eccrine Sweat Glands. *Lab Chip* **2017**, *17* (15), 2572–2580.

(22) Lin, B.; Sun, T.; Hui, J.; Zhou, L.; Xing, Z.; Wu, Z.; Mao, H. Monitoring of Sweat Ions and Physiological Parameters via a Reconfigurable Modular System. *ACS Sens.* **2024**, *9* (3), 1272–1279.

(23) Ursem, R. F. R.; Steijlen, A.; Parrilla, M.; Bastemeijer, J.; Bossche, A.; Wael, K. D. Worth Your Sweat: Wearable Microfluidic Flow Rate Sensors for Meaningful Sweat Analytics. *Lab Chip* **2025**, *25* (5), 1296–1315.

Downloaded from pubs.acs.org/ascecg/article-pdf/14/40/18238/6858153/sc-2026-07506n.pdf by TU DELFT user on 27 October 2026

https://doi.org/10.1021/acssuschemeng.6c07506
ACS Sustain. Chem. Eng. 2026, 14, 18238–18247